REVISTA MATÉRIA V.31
ISSN 1517-7076 articles e20260258, 2026

In situ generated SiC_w-ZrO_2 collaborative enhancing Al_2O_3-based composites and their mechanical properties

Kai Deng[1], Yuping Zhao[2], Aimin Chu[1], Henan Tu[1], Zhiqian Wang[1]

[1]Hunan University of Science and Technology, School of Materials Science and Engineering. 411201, Xiangtan China.

[2]Hunan University of Science and Technology, School of Civil and Engineering. 411201, Xiangtan, China.

e-mail: 23011901008@mail.hnust.edu.cn, 1020090@hnust.edu.cn, chuaiminme@163.com, 2420010211@mail.hnust.edu.cn, 121402243@qq.com

ABSTRACT

In this work, a four-step process was developed to fabricate Al_2O_3-based composites synergistically reinforced with in situ generated ZrO_2 and SiC_w. First, a homogeneous $Al_2O_3/SiO_2/ZrO_2$+C precursor was prepared by SCS method. Second, the precursor was converted into $Al_2O_3/SiC_w/ZrO_2$ composite powder through carbothermal reduction, water washing, and air calcination. Third, the composite powder was first mixed with a PVA solution by ball milling, and the resulting mixtures were then pressed into form a green compact of $Al_2O_3/SiC_w/ZrO_2$. Finally, the green compact were sintered by the APS method to obtain five $Al_2O_3/SiC_w/ZrO_2$ composites (denoted as ASxZy). The mechanical properties and wear resistance of the five ASxZy samples were investigated. The results indicate that the friction coefficients of the five ASxZy samples range from 0.6 to 0.7. Among them, the AS10Z20 sample exhibits the lowest wear rate and the best overall mechanical properties. In these ASxZy samples, SiC_w mainly inhibits crack propagation and dissipates fracture energy through whisker bridging, whisker pull-out, and crack deflection, whereas ZrO_2 mainly contributes to toughening through crack deflection and microcrack toughening. The dominant wear mechanism of four SiC_w-containing ASxZy samples is fatigue wear, whereas that of the AZ30 sample without SiC_w is adhesive wear.

Keywords: $Al_2O_3/SiC_w/ZrO_2$ composites; Mechanical properties; Wear resistance; SiC_w/ZrO_2 collaborative enhancement; Solution combustion synthesis.

1. INTRODUCTION

Al_2O_3 ceramics exhibit high hardness, high flexural strength, high wear resistance, and excellent chemical stability, and are widely used in fields such as machinery, electronics, and biomedical devices [1–4]. However, brittleness is a major drawback of Al_2O_3 ceramics, which shortens their service life and greatly limits their broader applications. Therefore, improving the fracture toughness of Al_2O_3 ceramics is of great importance for extending their service life and broadening their applications. The fracture toughness of Al_2O_3 ceramics is commonly improved by the following five strategies: (1) particle reinforcement using Cu, Si_3N_4, and SiC particles (SiC_p) [5–7], etc; (2) phase-transformation toughening, such as zirconia (ZrO_2) [8–10]; (3) one-dimensional reinforcement toughening, such as whiskers [11], fibers [12, 13], carbon nanotubes [14], and graphene [15], etc; (4) in-situ growth toughening [16, 17]; (5) synergistic toughening through multiphase-particle, whisker-particle interactions, and whisker/phase-transformation synergy [18–20].

Among these strategies, synergistic toughening is currently one of the most widely used toughening strategies and is also a promising future direction because it can take full advantage of multiple toughening mechanisms. However, in the fabrication of toughened Al_2O_3 ceramics, the traditional mechanical mixing methods tend to result in compositional inhomogeneity, particularly in whisker-reinforced systems. Whiskers are prone to entanglement and segregation within the matrix, which prevents them from fully exerting their toughening and reinforcing effects and thereby compromising the mechanical properties of Al_2O_3 ceramics [16]. The in-situ generation of whisker and particulate reinforcements in Al_2O_3 ceramics can effectively alleviate compositional inhomogeneity.

In this work, in-situ-generated SiC whiskers (SiC_w) and ZrO_2 particles were introduced into reinforce Al_2O_3 ceramics through a four-step process. The aim of this work was to address compositional inhomogeneity,

Corresponding Author: Aimin Chu Received on: 23/03/2026 Accepted on: 10/06/2026

DOI: https://doi.org/10.1590/1517-7076-RMAT-2026-0258

fully exploit the synergistic toughening effect of SiC_w and ZrO_2, and fabricate high-performance SiC_w/ZrO_2-reinforced Al_2O_3-based composites. Furthermore, the effects of the SiC_w/ZrO_2 ratio on the mechanical properties and wear resistance of the Al_2O_3-based composites were investigated in detail.

2. EXPERIMENTAL DETAILS

2.1. Experimental raw materials

The starting materials, including $ZrO(NO_3)_2$ (as the ZrO_2 source and oxidizer), $Al(NO_3)_3$ (as the Al_2O_3 source and oxidizer), silica gel (as the SiO_2 source), $CO(NH_2)_2$ (reducing agent), NaCl and NaF (growth aids), and $C_6H_{12}O_6$ (carbon source), were of analytical reagent grade. In all experiments, the amount of aluminum nitrate was fixed at 0.1 mol. The optimized molar ratio of urea to aluminum nitrate was 3:1. In all samples, the molar ratio of NaCl to $Al(NO_3)_3$ was 0.2:1, while the molar ratio of NaCl to NaF was 10:1. The amount of $C_6H_{12}O_6$ was optimized according to the atomic ratio of carbon to aluminum, which was set at 8. The amounts of silica gel and $ZrO(NO_3)_2$ were determined according to Table 1.

2.2. Preparation process of $Al_2O_3/SiC_w/ZrO_2$ composite materials

Figure 1 schematically illustrates the preparation process of $Al_2O_3/SiC_w/ZrO_2$ composites, which consists of the following four steps. (a) First, the starting materials were weighed according to the designed compositions and placed in a 1000 mL beaker. Then, 300 mL of deionized water was added, and the mixture was stirred with a glass rod until all the raw materials were completely dissolved. The beaker was placed on an electric furnace and heated at 300 °C to evaporate the solution. After solvent evaporation and concentration, a combustion reaction was triggered, releasing a large amount of heat and gas, which produced a loose precursor powder of $Al_2O_3/SiO_2/ZrO_2$/C/NaCl/NaF via solution combustion synthesis method (SCS). (b) Second, the precursor powder was placed in a tube furnace. Argon was used as the protective gas at a flow rate of 0.1 L/min. After being held at 1450 °C for 3 h, SiC whiskers (SiC_w) [21] and ZrC particles [22] were generated in situ, forming a composite powder composed of Al_2O_3/SiC_w/ZrC and residual C/NaCl/NaF. The NaCl/NaF system acted as a growth aid and played an important role in the growth of SiC_w during the heat treatment at 1450 °C by acting as a molten salt medium for reactant transport at high temperature, enhancing contact and mass transfer among reactants, lowering the reaction temperature, and improving the reaction efficiency [23]. Subsequently, the mixed powder was first washed with deionized water to remove residual NaCl/NaF, and then calcined at 700 °C in air for 1 h to remove residual carbon and meanwhile convert ZrC into ZrO_2 according to Equations (1) and (2) respectively, thereby obtaining pure $Al_2O_3/SiC_w/ZrO_2$ composite powder. It is worth noting that SiC_w remained resistant to oxidation during calcination in air owing to its high oxidation resistance [21]. (c) Third, because of the poor formability of the $Al_2O_3/SiC_w/ZrO_2$ composite powder, a 10 wt% PVA solution was added as a binder, and the resulting mixture was thoroughly stirred and homogenized by ball milling. After the solvent evaporated, the $Al_2O_3/SiC_w/ZrO_2$ composite powder was placed into a mold and pressed at 450 MPa and held for 120 s to form a green compact. (d) Finally, the green compact was first heated to 500 °C in a vacuum high-temperature furnace for 1 h to remove PVA. They were then sintered by atmospheric-pressure sintering (APS) method in the same high-temperature furnace to obtain $Al_2O_3/SiC_w/ZrO_2$ composites with various SiC_w/ZrO_2 ratios (ASxZy), as listed in Table 1. The optimized APS temperature and holding time were 1850 °C and 90 min, respectively. The flow rate of argon was 1 L/min, and the heating rate was set at 10 °C/min. After the holding period was completed, all samples were naturally cooled to room temperature in the furnace.

$$C + O_2 \rightarrow CO_2 \quad (1)$$

$$ZrC + 2O_2 \rightarrow ZrO_2 + CO_2 \quad (2)$$

Table 1: $Al_2O_3/SiC_w/ZrO_2$ composites with various S/Z (ASxZy).

MATERIAL NUMBER	Al_2O_3	SiC_w	ZrO_2
AS30	70	30	0
AS20Z10	70	20	10
AS15Z15	70	15	15
AS10Z20	70	10	20
AZ30	70	0	30

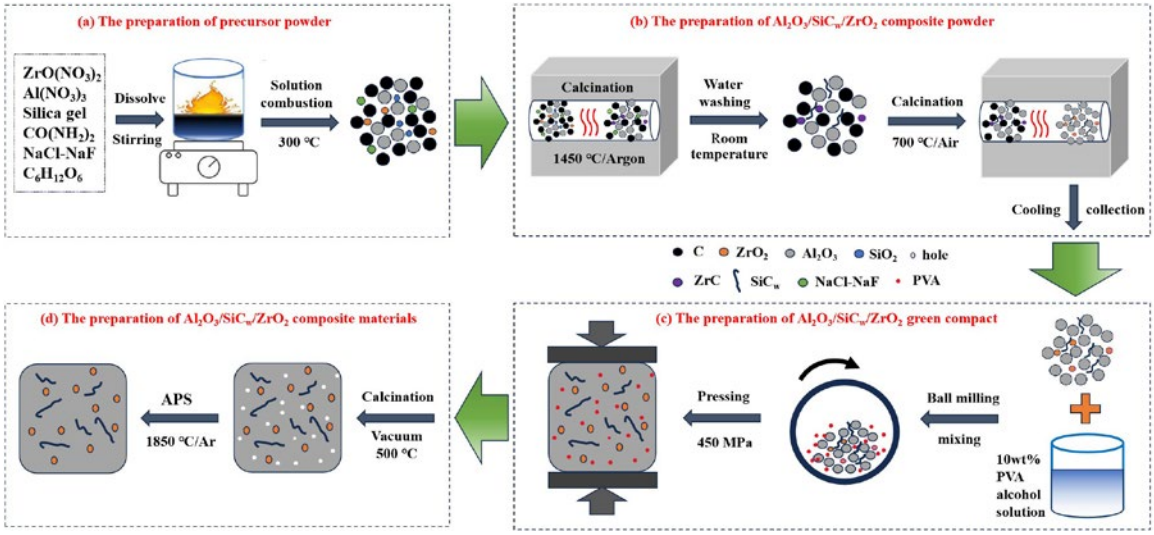

Figure 1: Preparation process for $Al_2O_3/SiC_w/ZrO_2$ composites.

2.3. Sample characterization and performance testing

XRD patterns of the samples were recorded using an X-ray diffractometer (D/max-RB12) with Cu Kα radiation. The morphology and particle size of the samples were observed using a scanning electron microscope (SEM, JSM-6380LV). The hardness of the five ASxZy samples was measured using a Vickers hardness tester (HV-30). The Vickers hardness test was conducted under a load of 196.0 N for 15 s, and the reported value was the average of five separate measurements.

Wear tests were conducted on five ASxZy samples with dimensions of 2 mm × 10 mm × 10 mm using a high-speed reciprocating wear tester with a ball-on-disk configuration (HSR-2M). The wear test conditions were as follows: a Si_3N_4 ball with a diameter of 5 mm and a hardness of 60 HRC was used as the counterface; the applied load was 8 N; the rotational speed was 400 r/min; the test duration was 20 min; the stroke length was 5 mm; the test temperature was 23 °C; and the relative humidity was 30%. The samples were cleaned with ethanol before and after the wear test, and the mass loss was measured using an electronic balance (model AB304-S). The wear rate was expressed in terms of wear volume, as shown in Equation (3).

$$V = W_{loss}/PS\rho \tag{3}$$

In Equation (3), V is the wear volume of the sample ($cm^3/N.m$); W_{loss} is the mass loss of the sample (mg); P is the applied normal load (N); S is the sliding distance (m); ρ is the theoretical density of the sample (g/cm^3).

The fracture toughness (K_{IC}) of five ASxZy samples was evaluated by the indentation method [24, 25], as shown in Equation (4). Here H is the indentation hardness, P is the indentation load, and L is the total crack length (mm). For each sample, 15 indentations were made at different positions, and the average value of these obtained results was taken as the fracture toughness of the sample.

$$K_{IC} = 0.0028\ (HP/L)^{1/2} \tag{4}$$

3. RESULTS AND DISCUSSION

3.1. Characterization of $Al_2O_3/SiC_w/ZrO_2$ composite powders

Figure 2 presents the XRD patterns of $Al_2O_3/SiC_w/ZrO_2$ composite powders with different S/Z ratios. As shown in Figure 2, only the diffraction peaks corresponding to SiC, ZrO_2, and Al_2O_3 were detected in the AS20Z10, AS15Z15, and AS10Z20 samples, and no impurity peaks were detected. This indicates that the reactants were completely converted and that high-purity $Al_2O_3/SiC_w/ZrO_2$ composite powders were successfully prepared. Figure 2 also showed that only the diffraction peaks of SiC and Al_2O_3 were observed in the AS30 sample, whereas only the diffraction peaks of ZrO_2 and Al_2O_3 were observed in the AZ30 sample. These results indicate that the target phases were successfully formed in both AS30 and AZ30.

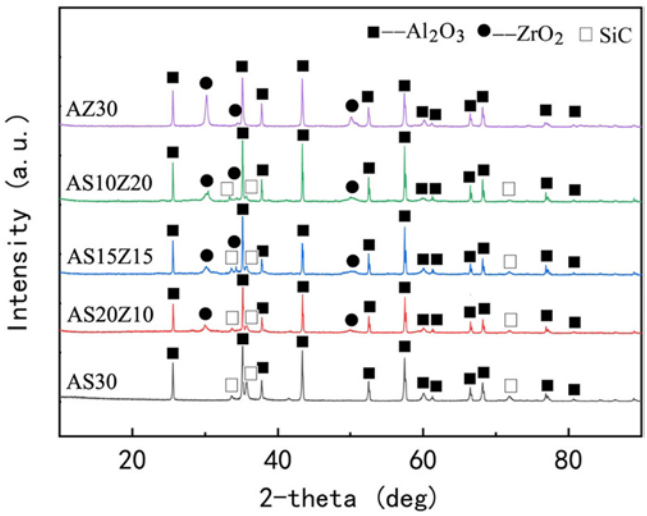

Figure 2: XRD patterns of $Al_2O_3/SiC_w/ZrO_2$ composite powders with various S/Z.

Figure 3 presents SEM images of $Al_2O_3/SiC_w/ZrO_2$ composite powders with different S/Z ratios. As shown in Figure 3a and b, a large number of slender SiC_w are observed in the AS30 and AS20Z10 samples. These whiskers are entangled with Al_2O_3/ZrO_2 particles measuring 5–8 μm and are interlaced and relatively uniformly distributed among the particles. The SiC_w are typically approximately 10 μm in length and 100–200 nm in diameter, indicating a high aspect ratio. It is worth noting that the number density of SiC_w in AS20Z10 decreases slightly compared with that in AS30. Figure 3c further shows that, with a decrease in the SiO_2 content, the number of SiC_w formed in AS15Z15 decreases significantly compared with those in AS20Z10 and AS30. Moreover, the whiskers become shorter and thicker, and some of them coalesce and grow in the same direction. A decrease in the aspect ratio of whiskers is beneficial to the densification of composite materials [26].

During the growth of SiC_w, molten NaCl/NaF at high-temperature acts as the mass-transfer medium. When the amount of the NaCl/NaF growth additive is kept constant, the amount of SiO_2 dissolved in the molten NaCl/NaF phase decreases as the SiO_2 content reducing, resulting in increased droplet fluidity. Therefore, the probability of contact between the generated SiC_w increases markedly, leading to simultaneous growth and partial coalescence, as shown in Figure 3c. This may lead to a less uniform distribution of SiC_w in the matrix. Compared with AS30 (Figure 3a), the whisker morphology becomes more irregular, and the SiC_w tends to become shorter and thicker. This is mainly because the decrease in the SiO_2 raw material available for SiC_w synthesis, and makes it difficult for the whiskers to continuously obtain sufficient SiO_2 during growth, thereby inhibiting further whisker growth.

As shown in Figure 3d, with a further decrease in SiO_2 content, the size of the SiC_w decreases significantly in AS10Z20. Most of the whiskers are short and curved, with lengths of about 2 μm, and are uniformly distributed within the Al_2O_3 matrix. Meanwhile, a small fraction of SiC_w with lengths of 5–10 μm is still present. As the relative content of NaCl/NaF increases, the transport rate of the NaCl/NaF droplets is accelerated, and the growth rate of SiC_w becomes controlled by the nucleation rate of silicon carbide. These factors may cause reactant accumulation at the growth front of SiC_w and an increase in supersaturation, thereby destabilizing SiC_w growth and causes whisker distortion [25]. Based on the above analysis, it can be concluded that the target composite powders can be successfully obtained by the present in-situ synthesis method, and that SiC_w and ZrO_2 can be uniformly distributed in the Al_2O_3 matrix. Moreover, as the SiO_2 content decreases, the length and aspect ratio of SiC_w decreases markedly, and the whisker morphology transforms from a long and straight shape to a short and coiled one.

3.2. Fracture morphology and mechanical properties of ASxZy

Figure 4 shows the fracture morphologies of the five $Al_2O_3/SiC_w/ZrO_2$ composites. It can be seen that AS15Z15 exhibits the largest grain size, with an average grain size of approximately 20 μm, whereas AZ30 shows the smallest grain size, approximately 10 μm. This is because AZ30 only underwent the first step, namely the solution combustion synthesis process, and its initial particle size was relatively small; therefore, grain growth during the APS process was limited. In contrast, the other four SiC_w-containing composite powders (AS30, AS20Z10,

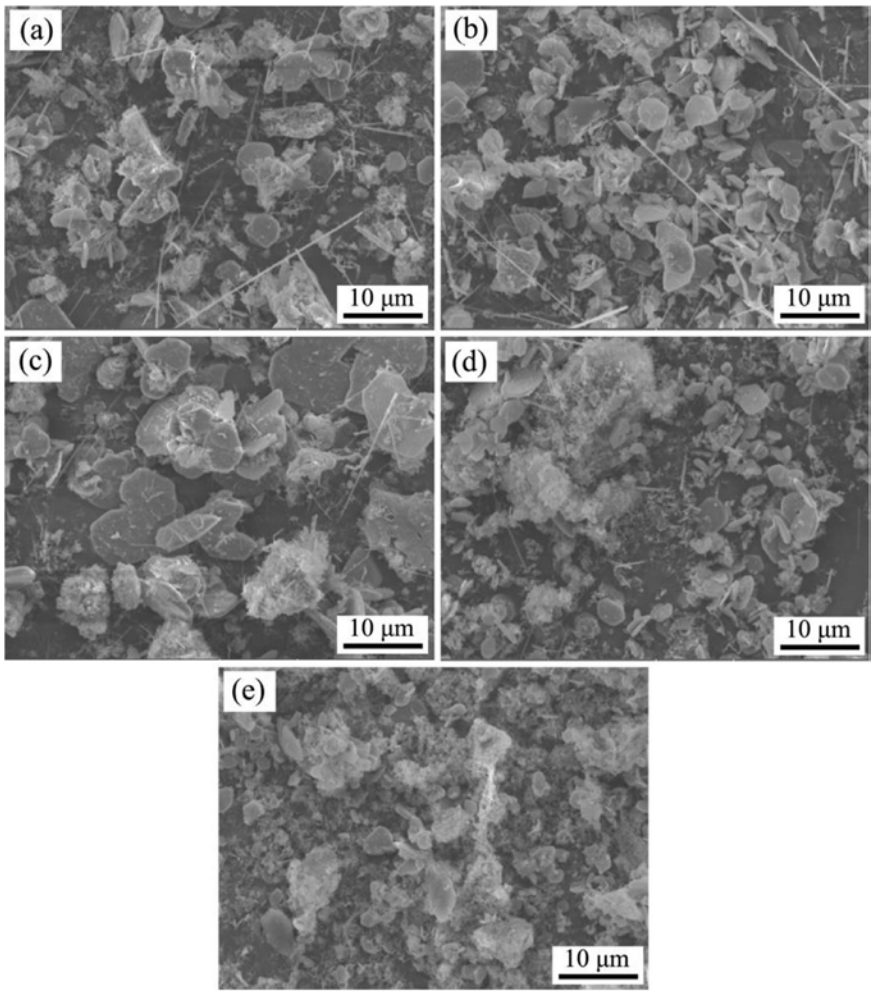

Figure 3: SEM images of $Al_2O_3/SiC_w/ZrO_2$ composite powders with various S/Z: (a) AS30; (b) AS20Z10; (c) AS15Z15; (d) AS10Z20; (e) AZ30.

AS15Z15, and AS10Z20) underwent not only the first step but also a second step involving high-temperature carbothermal reduction and calcination in air. These additional treatments promoted particle growth, and the grains further coarsened during the subsequent APS process. However, compared with AS15Z15 and AS10Z20 (Figure 4c and d), AS30 and AS20Z10 (Figure 4a and b) exhibit slightly smaller grain sizes, indicating that SiC_w has an inhibitory effect on matrix grain growth during processing. Moreover, due to the relatively higher SiC_w content in AS30 and AS20Z10, pores are more likely to form in the Al_2O_3 matrix under the same APS conditions, as shown in Figure 4a and b, resulting in insufficient intergranular bonding strength. Furthermore, the fracture surfaces of all the samples exhibit clear grain boundaries and relatively intact grains, indicating that their fracture modes are dominated by intergranular fracture.

Figure 5 shows the Vickers hardness of the five $Al_2O_3/SiC_w/ZrO_2$ composites. AS30 exhibits the lowest Vickers hardness, with a value of 15.2 GPa. As the SiC_w content decreases and the ZrO_2 content increases, the Vickers hardness of ASxZy gradually increases, as observed for AS20Z10. Because of the poor sinterability of SiC_w with the Al_2O_3 matrix, the SiC_w-containing samples are difficult to densify during the APS process, resulting in increased porosity. Therefore, a high SiC_w content leads to insufficient densification of the ASxZy samples, and the hardness is significantly lower than that expected for fully dense composites. However, although the SiC_w content decreases and the ZrO_2 content increases, a significant decrease in hardness is observed in AS15Z15. This is because, during the preparation of $Al_2O_3/SiC_w/ZrO_2$ composite powders, the growth of SiC_w was insufficient, and some whiskers became thick and coarse due to coalescence, resulting in a low aspect ratio. Meanwhile, SiC_w segregation caused structural inhomogeneity and increased porosity after APS, which led to a decrease in hardness. In addition, the hardness of the SiC_w-free AZ30 sample is also significantly lower. Therefore, AS10Z20 exhibits the highest hardness (17.4 GPa) among five samples, which can be attributed to the synergistic strengthening effect arising from the appropriate proportion of SiC_w and ZrO_2.

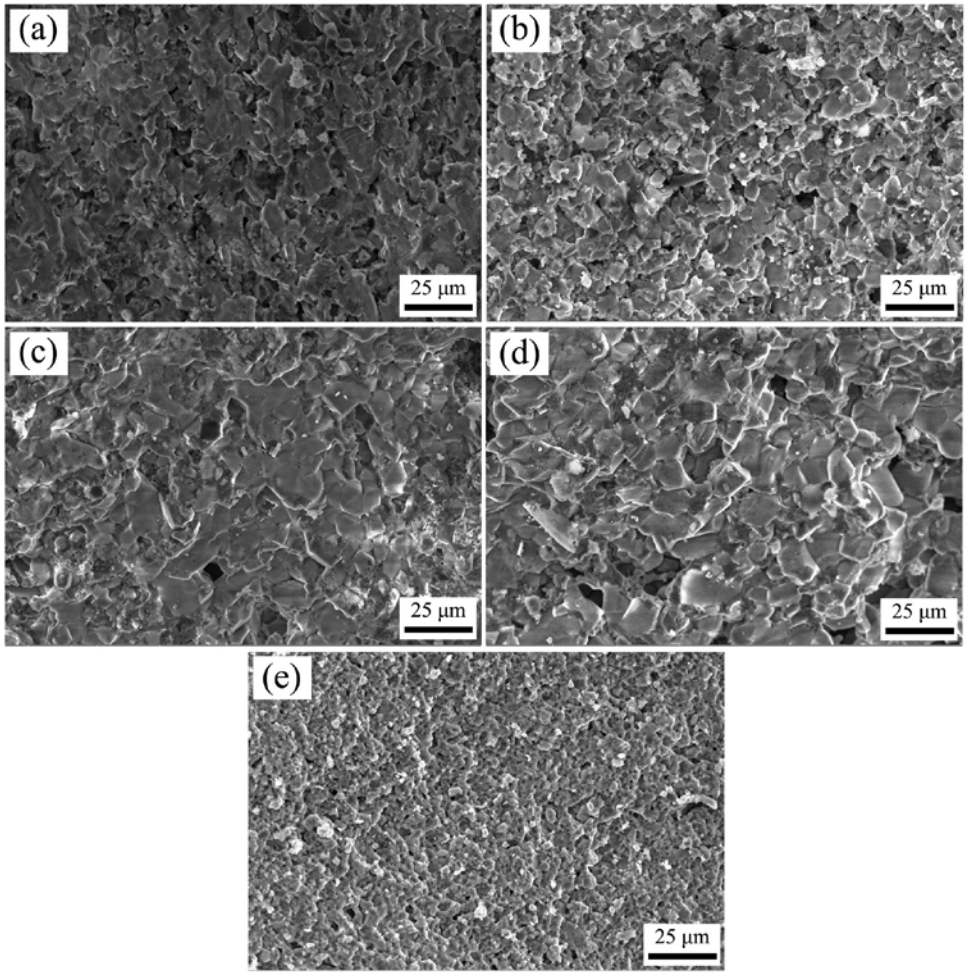

Figure 4: Fracture morphologies of the five $Al_2O_3/SiC_w/ZrO_2$ composites prepared by atmospheric-pressure sintering: (a) AS30; (b) AS20Z10; (c) AS15Z15; (d) AS10Z20; (e) AZ30.

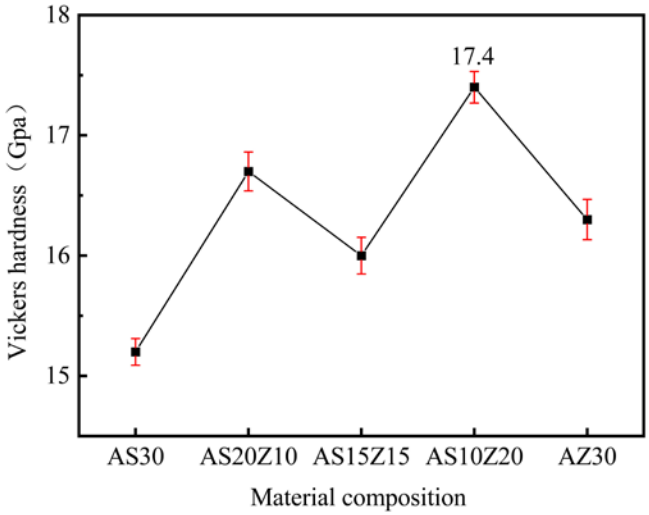

Figure 5: Vickers hardness of the five $Al_2O_3/SiC_w/ZrO_2$ composites prepared by atmospheric-pressure sintering.

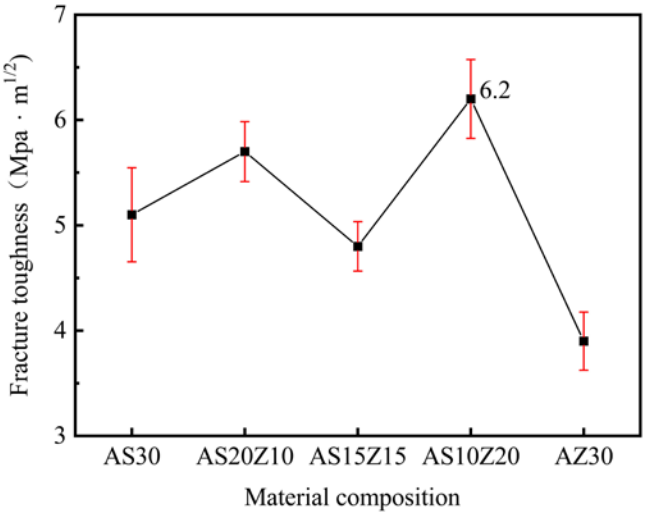

Figure 6: Fracture toughness of the five $Al_2O_3/SiC_w/ZrO_2$ composites prepared by atmospheric-pressure sintering.

Figure 6 shows the fracture toughness of the five $Al_2O_3/SiC_w/ZrO_2$ composites. The fracture toughness of the AZ30 sample without SiC_w addition is only 3.9 MPa·m$^{1/2}$, which is the lowest among the five samples and only slightly higher than that of pure alumina ceramics (3.79 MPa·m$^{1/2}$) owing to the toughening effect of ZrO_2 particles [27]. Figure 6 also shows that, compared with AZ30 without SiC_w addition, the other ASxZy samples containing SiC_w exhibit significantly improved fracture toughness, the SiC_w acted as a load-bearing and crack-bridging phase, thereby improving the fracture toughness of the ceramic matrix through crack bridging, pull-out, and deflection [28]. However, the toughening effect is also influenced by the APS conditions and the morphology of the composite powders. For example, AS15Z15 failed to fully exploit the toughening role of SiC_w, and its fracture toughness was only 4.8 MPa·m$^{1/2}$. In general, the fracture toughness of Al_2O_3-based composites tends to increase with increasing whisker content [29]. However, in the AS30 and AS20Z10 samples, the high SiC_w content makes it difficult to achieve sufficient interfacial bonding between SiC_w and the Al_2O_3 matrix during APS, thereby limiting the toughening effect of SiC_w [30]. Therefore, the fracture toughness values of AS30 and AS20Z10 are 5.1 MPa·m$^{1/2}$ and 5.7 MPa·m$^{1/2}$, respectively. Moreover, AS10Z20 contains a relatively low amount of SiC_w, and the prepared composite powders have a relatively uniform particle sizes. In addition, most of the SiC_w are uniformly distributed in the matrix (Figure 3d). Under these conditions, SiC_w can form effective interfacial bonding with the Al_2O_3 matrix, and suppress matrix grain growth during APS, and effectively contribute to toughening. On one hand, some t-ZrO_2 particles in AS10Z20 transformed into m-ZrO_2 spontaneously, which weakened the shielding effect of the crack tip when the specimens were loaded. On the other hand, the large difference in the thermal expansion coefficient made ZrO_2 bear higher tensile stress. Furthermore, semi-coherent interfaces may form at the ZrO_2/Al_2O_3, Al_2O_3/SiC_w, and ZrO_2/SiC_w phase boundaries, which is beneficial for increasing the resistance to crack propagation, consequently improving the fracture toughness [31]. Therefore, the fracture toughness of the AS10Z20 sample reaches the highest value of 6.2 MPa·m$^{1/2}$ in the present work. However, this value is slightly lower than the value of 6.67 MPa·m$^{1/2}$ reported by ZHANG *et al.* [32]. Compared with the APS method used in present work, the oscillatory pressure sintering (OPS) method adopted in reference 32 can effectively eliminate agglomerated pores and reduce pore size and number, thereby improving fracture toughness.

Figure 7 shows the friction coefficients and wear rates of the five $Al_2O_3/SiC_w/ZrO_2$ composites. As shown in Figure 7, the friction coefficients of all five samples fall within the range of 0.6–0.7. Since the matrix is mainly composed of Al_2O_3, the fluctuation in friction coefficient is relatively small [27]. However, the wear rates of the five samples vary significantly, which can be attributed to the different contents of added SiC_w and ZrO_2. Because AS30 contains the highest amount of SiC_w, it exhibits the poorest wear resistance under the same APS conditions. Moreover, its interfacial bonding strength is insufficient, because SiC_w is prone to detachment under load. In contrast, AS10Z20 exhibits the lowest wear rate (2.36×10^{-10} cm^3/N·m) among the five samples, indicating that an appropriate proportion of added SiC_w/ZrO_2 can produce a synergistic strengthening effect.

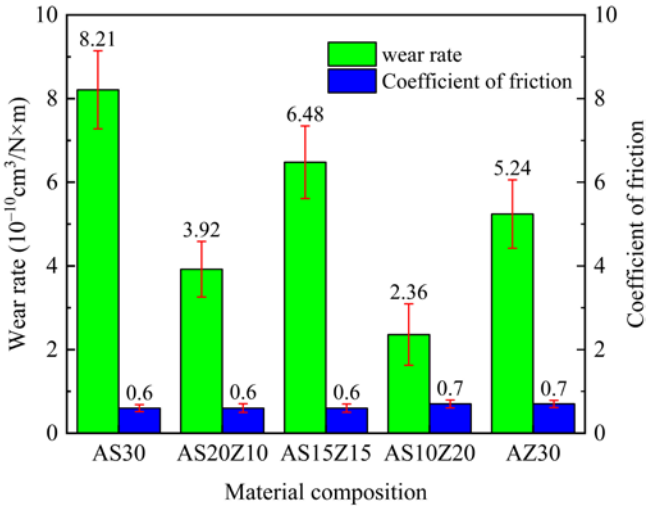

Figure 7: Wear rate and friction coefficient of the five $Al_2O_3/SiC_w/ZrO_2$ composites prepared by atmospheric-pressure sintering.

Figure 8 shows SEM images of the worn surfaces of the five $Al_2O_3/SiC_w/ZrO_2$ composites. As shown in the left image of Figure 8a, no large-scale peeling of the matrix is observed in AS30 because of the presence of numerous SiC_w. These whiskers act as bridges across cracks and suppress the peeling of the Al_2O_3 matrix. In addition, crack propagation is observed in the AS30 sample, as shown in the right image of Figure 8a. However, the right image of Figure 8a shows crack deflection and bridging phenomena during crack propagation, indicating that SiC_w hinders crack propagation and thereby suppressing peeling of the matrix surface. Furthermore, SiC_w hindered removal of pores at a higher concentration where the agglomeration of SiC_w occurred and formed the bridging effect that resulted in the highest wear rate of AS30, as shown in Figure 7. For AS20Z10, no severe detachment of the matrix surface is observed in the left image of Figure 8b. However, obvious local detachment can still be seen in some areas, as shown in the right image of Figure 8b. With the decrease in SiC_w content and the increase in ZrO_2 content, the bonding strength between SiC_w and the Al_2O_3 matrix is enhanced, and the densification behavior is correspondingly improved, thereby further strengthening the synergistic effect of SiC_w and ZrO_2 in the matrix. The left image of Figure 8c shows the worn surface morphology of AS15Z15. It can be observed from Figure 8c that a large number of pits formed on the matrix surface as a result of material peeling during wear, indicating that the reinforcing effect of SiC_w on the matrix was weakened. The coalescence and branching of some SiC_w can lead to poor dispersion of SiC_w in the Al_2O_3 matrix (see Figure 3c), which can cause SiC_w segregation and adversely affect the mechanical properties of the sample during the sintering process [25].

As shown in the left panel of Figure 8d, no evident matrix peeling is observed on the worn surface of AS10Z20 as the SiC_w content further decreases. This indicates that SiC_w effectively retards crack propagation in the matrix and hinders material detachment from the matrix surface [28]. The right panel of Figure 8d shows the propagation of microcracks. It can also be clearly observed from Figure 8d that the cracks are mainly deflected, which lengthens the crack propagation path and suppresses matrix detachment, thereby further reducing the wear rate. Figure 8e shows the worn surface morphology of AZ30. It can be clearly observed from Figure 8e that severe matrix peeling occurs during wear because of the absence of SiC_w, resulting in the detachment of large fragments from the matrix surface. Finally, Figure 8a-c show that the four ASxZy samples containing SiC_w exhibit a small number of cracks and some large pits on the matrix surface during wear, which are typical characteristics of fatigue wear. However, Figure 8e shows that no obvious cracks are observed in the AZ30 sample without SiC_w addition, whereas severe detachment of large pieces from the matrix surface occurs during wear, which is characteristic of adhesive wear.

4. CONCLUSION

$Al_2O_3/SiC_w/ZrO_2$ composite powders with various S/Z ratios were first prepared in the present work by combining solution combustion synthesis with carbothermal reduction. These composite powders were then sintered using the atmospheric-pressure sintering (APS) method to obtain $Al_2O_3/SiC_w/ZrO_2$ composites with various S/Z

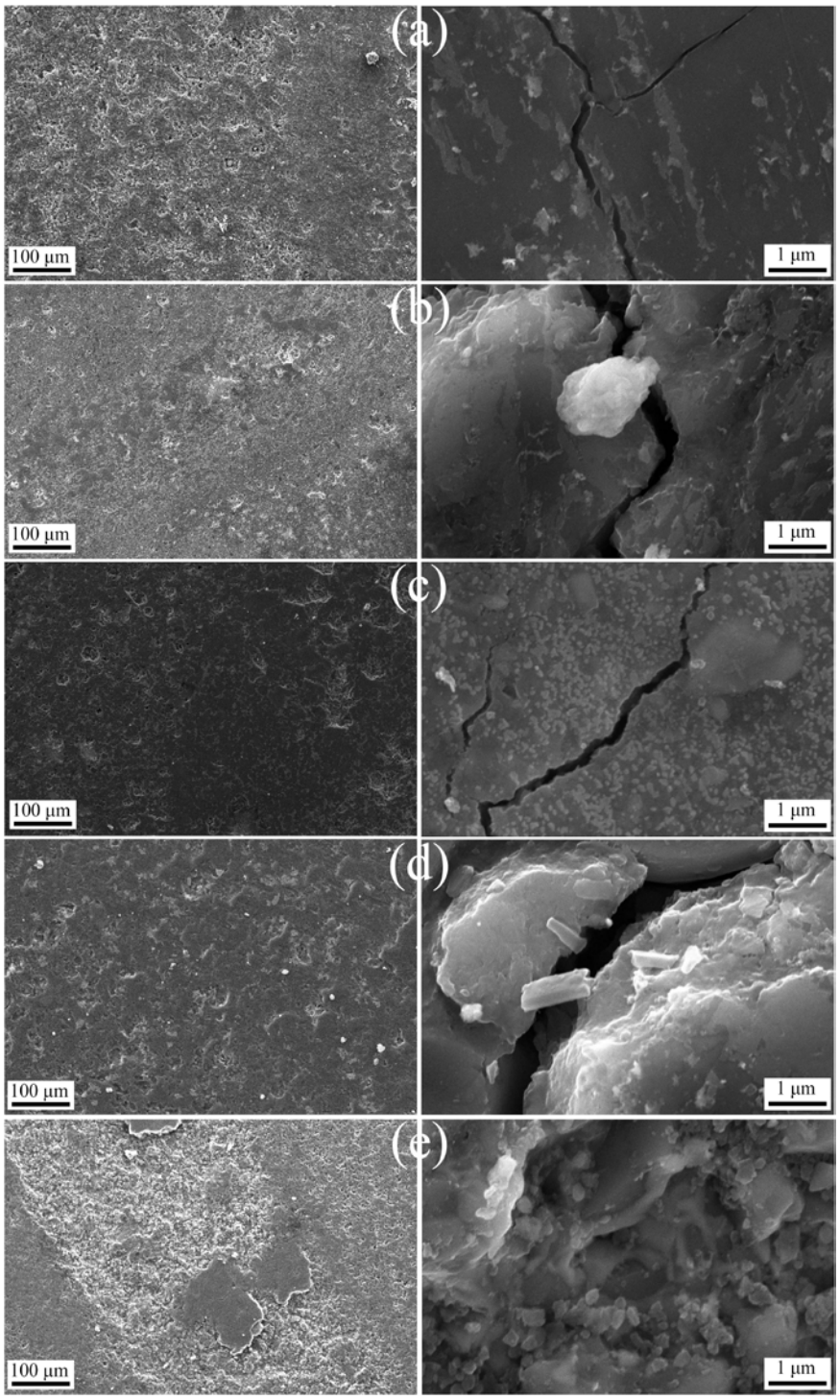

Figure 8: SEM images of the worn surfaces of the five $Al_2O_3/SiC_w/ZrO_2$ composites prepared by atmospheric-pressure sintering: (a) AS30; (b) AS20Z10; (c) AS15Z15; (d) AS10Z20; (e) AZ30.

ratios (ASxZy). The mechanical properties and wear resistance of the ASxZy samples were tested, and their fracture and wear mechanisms were analyzed. The main conclusions are as follows.

(1) During the preparation of $Al_2O_3/SiC_w/ZrO_2$ composite powders with various S/Z ratios, it was found that, as the SiO_2 content decreased and the relative increase in NaCl/NaF content, the morphology of the generated SiC_w gradually changed from a long and straight shape (such as AS30 and AS20Z10) to a short and curved one (such as AS15Z15 and AS10Z20).

(2) Among the five ASxZy samples, AZ30 exhibits the smallest grain size of approximately 10 μm. This is because AZ30 only underwent the solution combustion synthesis step before APS, and its initial particle size was relatively small, therefore, grain growth during the APS process was limited. In contrast, AS15Z15 exhibits the largest grain size of approximately 20 μm and shows a fracture mode dominated by intergranular fracture.

(3) Among the five ASxZy samples, AS10Z20 exhibits the highest hardness and fracture toughness (17.4 GPa, 6.2 $MPa \cdot m^{1/2}$), as well as the lowest wear rate (2.36×10^{-10} $cm^3/N \cdot m$).

(4) The wear mechanism of the four ASxZy samples containing SiC_w is mainly fatigue wear, whereas that of the AZ30 sample without SiC_w addition is mainly adhesive wear.

Although AS10Z20 exhibits the best comprehensive performance in the present work, there is still significant room for improvement in its density and mechanical properties. In order to improve the mechanical properties of AS10Z20, the focus of our future work is to conduct research on advanced sintering methods such as spark plasma sintering (SPS) or oscillatory pressure sintering (OPS), et al, as well as the influence of the size of SiC_w and zirconia particles on the microstructure and properties of the sintered composites.

5. ACKNOWLEDGMENTS

This work is financially supported by National Natural Science Foundation Program of China (52174344), Natural Science Foundation Program of Hunan (2024JJ7178).

6. DATA AVAILABILITY

The data that support the findings of this study are available from the corresponding author upon reasonable request.

7. BIBLIOGRAPHY

[1] CABRAL, R.F., LOURO, L.H.L., CAMPOS, J.B., *et al.*, "Efeito da adição de Nb_2O_5 na sinterização de Al_2O_3-Y_2O_3", *Matéria*, v. 19, n. 2, pp. 125–131, Apr. 2014. doi: https://doi.org/10.1590/S1517-70762014000200007.

[2] DEJA, M., ZIELINSKI, D., AGEBO, S.W., "Study on the wear characteristics of a 3D printed tool in flat lapping of Al_2O_3 ceramic materials", *Wear*, v. 556–557, pp. 205515, Jul. 2024. doi: https://doi.org/10.1016/j.wear.2024.205515.

[3] LI, C., LAI, C., WU, Y., *et al.*, "CMAS corrosion resistance of Y_2O_3–Al_2O_3 binary ceramic materials", *Ceramics International*, v. 50, n. 8, pp. 13721–13731, Jan. 2024. doi: https://doi.org/10.1016/j.ceramint.2024.01.286.

[4] WANG, X., ZHONG, Y., HU, Q., "A review of Al_2O_3-based eutectic ceramics for high-temperature structural materials", *Journal of Materials Science and Technology*, v. 214, pp. 214–232, Jul. 2025. doi: https://doi.org/10.1016/j.jmst.2024.07.012.

[5] OH, S.T., SEKINO, T., NIIHARA, K., "Fabrication and mechanical properties of 5vol% copper dispersed alumina-nanocomposite", *Journal of the European Ceramic Society*, v. 18, n. 1, pp. 31–37, Jan. 1998. doi: https://doi.org/ 10.1016/S0955-2219(97)00099-X.

[6] BAI, X., HUANG, C., WANG, J., *et al.*, "Fabrication and characterization of Si_3N_4 reinforced Al_2O_3-based ceramic tool materials", *Ceramics International*, v. 41, n. 10, pp. 12798–12804, Dec. 2015. doi: https://doi.org/10.1016/j.ceramint.2015.06.115.

[7] KUMAR, S.S., DEVAIAH, M., BAI, V.S., *et al.*, "Mechanical properties of SiC_p/Al_2O_3 ceramic matrix composites prepared by directed oxidation of an aluminum alloy", *Ceramics International*, v. 38, n. 2, pp. 1139–1147, Mar. 2012. doi: https://doi.org/10.1016/j.ceramint.2011.08.042.

[8] WANG, X., ZHONG, Y., SUN, Q., *et al.*, "Crystallography and interfacial structure in a directionally solidified $Al_2O_3/Y_3Al_5O_{12}/ZrO_2$ eutectic crystal", *Scripta Materialia*, v. 145, pp. 23–27, Mar. 2018. doi: https://doi.org/10.1016/j.scriptamat.2017.10.008.

[9] SOMMER, F., LANDFRIED, R., KERN, F., *et al.*, "Mechanical properties of zirconia toughened alumina with 10~24vol.%1Y-TZP reinforcement", *Journal of the European Ceramic Society*, v. 32, n. 16, pp. 4177–4184, Dec. 2012. doi: https://doi.org/10.1016/j.jeurceramsoc.2012.06.019.

[10] HASSAN, A.M., NAGA, S.M., AWAAD, M., "Toughening and strengthening of Nb_2O_5 doped zirconia/alumina (ZTA) composites", *International Journal of Refractory & Hard Metals*, v. 48, pp. 338–345, Jan. 2015. doi: https://doi.org/10.1016/j.ijrmhm.2014.10.006.

[11] TU, Z., LAO, X., XU, X., *et al.*, "One-step synthesis of Al_2O_3-β-Sialon nanowhiskers ceramics for fluid-bed thermal storage system of solar energy", *Next Nanotechnology*, v. 5, pp. 100039, 2024. doi: https://doi.org/10.1016/j.nxnano.2023.100039.

[12] JIANG, R., SUN, X., LIU, H., *et al.*, "Microstructure and mechanical properties improvement of the Nextel™ 610 fiber reinforced alumina composite", *Journal of the European Ceramic Society*, v. 41, n. 10, pp. 5394–5399, Aug. 2021. doi: https://doi.org/10.1016/j.jeurceramsoc.2021.04.031.

[13] HABLITZEL, M.P., GARCIA, D.E., HOTZA, D., "Interfaces fracas em compósitos de matriz cerâmica de alumina/alumina", *Matéria*, v. 16, n. 3, pp. 788–794, Feb. 2011. doi: https://doi.org/10.1590/S1517-70762011000300006.

[14] LIU, Y., RAMIREZ, C., ZHANG, L., *et al.*, "In situ direct observation of toughening in isotropic nanocomposites of alumina ceramic and multiwall carbon nanotubes", *Acta Materialia*, v. 127, pp. 203–210, Apr. 2017. doi: https://doi.org/10.1016/j.actamat.2017.01.024.

[15] LU, P., CHEN, H., ZHANG, J., *et al.*, "Effects of graphene pull-out on the interfacial mechanical properties of alumina/graphene nanocomposite ceramic tool materials: Molecular dynamics analysis and material preparation", *International Journal of Applied Ceramic Technology*, v. 21, n. 1, pp. 451–464, Aug. 2023. doi: https://doi.org/10.1111/ijac.14525.

[16] ZHU, J., XUE, Y., BAI, X., *et al.*, "Preparation of in situ growth multiscale-sialon grain-reinforced Al_2O_3-based composite ceramic tool materials", *Materials*, v. 16, n. 6, pp. 2333, Mar. 2023. doi: https://doi.org/10.3390/ma16062333. PubMed PMID: 36984209.

[17] SKTANI, Z.D.I., AZHAR, A.Z.A., RATNAM, M.M., *et al.*, "The influence of in-situ formation of hibonite on the properties of zirconia toughened alumina (ZTA) composites", *Ceramics International*, v. 40, n. 4, pp. 6211–6217, May. 2014. doi: https://doi.org/10.1016/j.ceramint.2013.11.076.

[18] CHEN, Z., JI, L., GUO, N., *et al.*, "Crack healing and strength recovery of Al_2O_3/TiC/TiB_2 ceramic tool materials", *International Journal of Refractory & Hard Metals*, v. 87, pp. 105167, Feb. 2020. doi: https://doi.org/10.1016/j.ijrmhm.2019.105167.

[19] VERMA, V., MANOJ, K., "Synthesis microstructure and mechanical properties of Al_2O_3/ZrO_2/CeO_2 composites with addition of Nickel and Titania processed by conventional sintering", *Materials Today: Proceedings*, v. 4, n. 2, pp. 3062–3071, 2017. doi: https://doi.org/10.1016/j.matpr.2017.02.189.

[20] EL-MEHALAWY, N., MANSOUR, T.S., TURKY, G.M., *et al.*, "Dielectric and thermo-mechanical evaluation of Nb_2O_5 doped ß-spodumene/alumina ceramic composite for high voltage insulation", *Journal of Alloys and Compounds*, v. 1046, pp. 184869, Nov. 2025. doi: https://doi.org/10.1016/j.jallcom.2025.184869.

[21] CHU, A., ZHANG, D., RAFI-UD-DIN, R., *et al.*, "Polyacrylamide-assisted combustion-carbothermal synthesis of well-distributed SiC nanowires", *Ceramics International*, v. 41, n. 10, pp. 14585–14591, Dec. 2015. doi: https://doi.org/10.1016/j.ceramint.2015.07.176.

[22] CHU, A., QIN, M., RAFI-UD-DIN, R., *et al.*, "Carbothermal synthesis of ZrC powders using a combustion synthesis precursor", *International Journal of Refractory & Hard Metals*, v. 36, pp. 204–210, Jan. 2013. doi: https://doi.org/10.1016/j.ijrmhm.2012.08.016.

[23] ZHANG, J., LI, W., JIA, Q., *et al.*, "Molten salt assisted synthesis of 3C-SiC nanowire and its hotoluminescence properties", *Ceramics International*, v. 41, n. 10, pp. 12614–12620, Dec. 2015. doi: https://doi.org/10.1016/j.ceramint.2015.06.089.

[24] JIANG, W., LU, H., CHEN, J., *et al.*, "Toughening cemented carbides by phase transformation of zirconia", *Materials & Design*, v. 202, pp. 109559, Apr. 2021. doi: https://doi.org/10.1016/j.matdes.2021.109559.

[25] SHI, F., YANG, D., TIAN, Y., *et al.*, "Indentation methods for evaluating fracture toughness in glass materials: A review", *Theoretical and Applied Fracture Mechanics*, v. 140, pp. 105195, Dec. 2025. doi: https://doi.org/10.1016/j.tafmec.2025.105195.

[26] SUN, L., PAN, J., "TiC whisker-reinforced $MoSi_2$ matrix composites", *Materials Letters*, v. 51, n. 3, pp. 270–274, Nov. 2001. doi: https://doi.org/10.1016/S0167-577X(01)00303-2.

[27] CAI, K.F., MCLACHLAN, D.S., AXEN, N., *et al.*, "Microstructure and properties of Al_2O_3-TiC composites", *Ceramics International*, v. 28, n. 2, pp. 217–222, Jan. 2002. doi: https://doi.org/10.1016/S0272-8842(01)00080-3.

[28] YIN, G., LI, W., JIANG, K., *et al.*, "Mechanical properties and high-velocity impact tests of SiC_w-reinforced Al_2O_3-ZrO_2 ceramic", *Ceramics International*, v. 51, n. 24, pp. 41547–41562, Oct. 2025. doi: https://doi.org/10.1016/j.ceramint.2025.06.379.

[29] BECHER, P.F., HSUEH, C., ANGELINI, P., *et al.*, "Toughening behavior in whisker reinforced ceramic matrix composites", *Journal of the American Ceramic Society*, v. 71, n. 12, pp. 1050–1061, Dec. 1988. doi: https://doi.org/10.1111/j.1151-2916.1988.tb05791.x.

[30] YOU, X.Q., SI, T.Z., LIU, N., *et al.*, "Effect of grain size on thermal shock resistance of Al_2O_3-TiC ceramics", *Ceramics International*, v. 31, n. 1, pp. 33–38, Jan. 2005. doi: https://doi.org/10.1016/j.ceramint.2004.02.009.

[31] ZHANG, J., ZHU, T., CHENG, Y., *et al.*, "Fabrication and mechanical properties of ZrO_2-Al_2O_3-$SiC_{(w)}$ composites by oscillatory pressure sintering", *Ceramics International*, v. 46, n. 16, pp. 25719–25725, Nov. 2020. doi: https://doi.org/10.1016/j.ceramint.2020.07.048.

[32] ZHANG, J., ZHU, T., SANG, S., *et al.*, "Microstructural evolution and mechanical properties of ZrO_2(3Y)-Al_2O_3-$SiC_{(w)}$ ceramics under oscillatory pressure sintering", *Materials Science and Engineering A*, v. 819, pp. 141445, Jul. 2021. doi: https://doi.org/10.1016/j.msea.2021.141445.